ACS OMEGA

Article

Cite This: ACS Omega 2018, 3, 2618−2627

Highly Pure Silica Nanoparticles with High Adsorption Capacity Obtained from Sugarcane Waste Ash

Suzimara Rovani,[†] Jonnatan J. Santos,*[,‡] Paola Corio,[‡] and Denise A. Fungaro[†]

[†]Instituto de Pesquisas Energéticas e Nucleares (IPEN-CNEN/SP), Av. Prof. Lineu Prestes, 2242, Cidade Universitária, 05508-000 São Paulo, São Paulo, Brazil

[‡]Instituto de Química, Universidade de São Paulo, Av. Prof. Lineu Prestes, 748, Cidade Universitária, P.O. Box 26077, 05508-000 São Paulo, São Paulo, Brazil

Supporting Information

ABSTRACT: Silica nanoparticles (SiO_2NPs) from renewable sources can be used in very different materials, such as paints, membranes for fuel cells, Li-ion batteries, adsorbents, catalysts, and so on. Brazil is the world's largest producer of sugarcane and generates huge amounts of sugarcane waste ash (SWA), which is a Si-rich source. This study investigates a method to produce highly pure SiO_2NPs from SWA. The SiO_2NPs were characterized by inductively coupled plasma optical emission spectroscopy, scanning and transmission electron microscopy (TEM), X-ray diffraction analyses, specific surface area and pore distribution, UV and Fourier transform infrared spectroscopy, and thermogravimetric analyses and applied as an adsorbent material in the removal of acid orange 8 (AO8) dye from aqueous solution. The SiO_2 content was 88.68 and 99.08 wt % for SWA and SiO_2NPs, respectively. TEM images of SWA and SiO_2NPs exhibit drastic alterations of the material size ranging from several micrometers to less than 20 nm. The SiO_2NPs showed a specific surface area of 131 $m^2\ g^{-1}$ and adsorption capacity of around 230 mg g^{-1} for acid orange 8 dye. Furthermore, the recycling of the SiO_2NPs adsorbent after AO8 adsorption was very satisfactory, with reuse for up to five cycles being possible. The results indicate that it was possible to obtain highly pure silica in a nanosize from the waste material and produce an adsorbent with high adsorption capacity and the possibility of reuse.

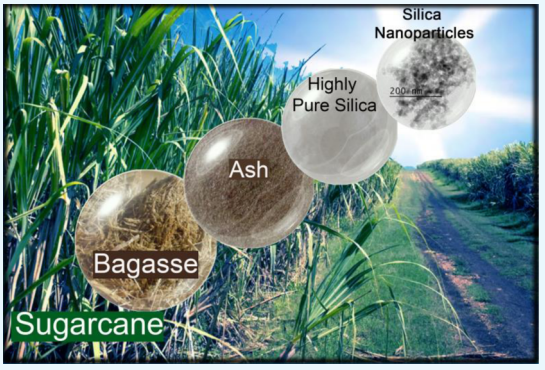

INTRODUCTION

Adding value to agroindustrial solid wastes, produced on a large scale, is a challenge for sustainable and green chemistry. Innovative and creative ways to reduce waste and the contamination of the environment, minimizing environmental impacts, have been targeted in the 21st century.[1−3] The largest agroindustrial by-products of the world are rice husk and straw, corn cobs, wheat straw, and sugarcane bagasse. Among these by-products, sugarcane bagasse and rice husk and straw can be highlighted because of their high silicon content, being important renewable sources.[4,5] However, only rice husk and ash are frequently found in the literature as renewable sources to produce value-added materials based on silicon, such as, silica nanoparticles (SiO_2NPs).[6−10]

There are still few studies about the use of sugarcane bagasse and ash as raw materials for the production of SiO_2NPs, opening up opportunities for this material.[4,11,12] In this sense, Brazil plays an important role, as it is the largest producer of sugarcane in the world, producing about 657 million tons per year,[13,14] specially utilized to produce sugar and ethanol, generating straw and bagasse as main wastes. These wastes are burned as fuel in boilers that generate the water vapor used in the production of sugar and ethanol and in energy cogeneration processes. After burning, about 3−12 million tons of ash/year are generated; this ash has negligible costs and is easily overlooked in landfills. Handling and improper disposal in places such as soil, water, and air can lead to pollution, which causes environmental problems and human health, especially when the silica present in the ash is in crystalline form. Ash from sugarcane residues presents Si as the main chemical element generally above 70% by mass.[15] Therefore, the development of new studies related to the use of this raw material rich in Si for the production of SiO_2NPs is fundamental. They have a wide range of applications in paints,[16] biopolymers,[17] membranes for fuel cells,[18] Li-ion batteries,[19] catalysts,[20] stationary phases for chromatographic columns,[2] and adsorbents,[21−23] among other applications.[24]

Adsorption has an important functionality in the environment, being considered one of the most promising techniques for treating waste water. The preparation of adsorbents utilizing agroindustrial waste generates a material known as green adsorbent. A good green adsorbent must be low cost and have satisfactory adsorption properties and the possibility of reuse.[25] Among the green adsorbents found in the literature, the main

Received: January 16, 2018
Accepted: February 22, 2018
Published: March 5, 2018

DOI: 10.1021/acsomega.8b00092
ACS Omega 2018, 3, 2618−2627

ones are activated carbon and biochar produced from agroindustrial waste.[26] However, SiO_2NPs produced from agroindustrial solid waste have also been applied as green adsorbents.[21−23] The success of the adsorption in wastewater processes depends on many factors, such as the high degree of porosity, the extensive internal surface area, and the favorable chemical surface of the adsorbents. Several studies already use SiO_2NPs for the adsorption of organic contaminants with success.[21−23,27]

Thus, in this study, SiO_2NPs were produced from sugarcane waste ash (SWA) and characterized by different techniques. These nanoparticles were applied as an adsorbent material for the removal of acid orange 8 dye from aqueous solution. The adsorption capacity and the reuse cycles of SiO_2NPs were also evaluated.

RESULTS AND DISCUSSION

Chemical and Structural Properties of SWA and SiO_2NPs. SWA raw, obtained by burning of sugarcane waste, can contain a lot of different impurities, especially salt and carbon species. The pretreatment procedure was performed aiming to eliminate excess salts, organic compounds, and low-solubility elements through washing and to eliminate particles with a size of more than 0.6 mm by sieve.[28]

After this pretreatment procedure, silicon was extracted from SWA by reaction with sodium hydroxide under heating at 400 °C, as adapted from the literature.[29] At 400 °C, sodium hydroxide is melted, which increases silicon extraction. This procedure helps to increase silicon purity, liberating elements which can be in the structure of ash, making them more soluble. This procedure of extraction generates silicon in the form of silicate, and after extraction, this silicate was solubilized in deionized water, filtered, and saved for the preparation of SiO_2NPs. Sodium silicate (Na_2SiO_3) solution density was estimated as 1.23 g cm^{-3} (determined by weighing ten times 1 mL of the solution mentioned and calculating the average) and its Si composition, as determined by gravimetric analyses, was estimated as 5.42 wt % (following the procedure as described in the literature[30]).

SiO_2NPs can be prepared by a wide variety of methods, including the sol−gel method, hydrothermal synthesis, flame synthesis, and the reverse microemulsion technique, and the functionalization of SiO_2NPs may be performed by grafting or co-condensation methods. In the co-condensation, the SiO_2NPs preparation and functionalization occurs in a single step and involves the hydrolysis−condensation reaction.[20,31,32]

In this study, the sodium silicate solution obtained was utilized to prepare SiO_2NPs, the production of SiO_2NPs is based on hydrolysis (production of silanol groups) and condensation (formation of siloxane) reaction using sulfuric acid in a biphasic medium in the presence of cetyltrimethylammonium bromide (CTAB).[20,33]

CTAB is a classical micelle maker and helps to control the size of nanoparticles, to prevent agglomeration, and to modify their surface as described in the literature.[20,31,32] This way, the co-condensation procedure using sulfuric acid generates a white solid with low dispersion in both media and easily removed by centrifugation.

After the separation of SiO_2NPs by centrifugation, the composition of elements present in SWA and SiO_2NPs obtained was determined by ICP−OES, (Table 1) and the morphology of SWA and SiO_2NPs was determined by scanning and transmission electron microscopy (SEM and TEM), as shown in Figure 1.

Table 1. Weight Percentages of Elements Present in Sugarcane Waste Ash and Silica Nanoparticle Samples Determined by Inductively Coupled Plasma Optical Emission Spectroscopy (ICP−OES)

elements	SWA (wt %)	SiO_2NPs (wt %)
[a]SiO_2	88.68	99.08
Al_2O_3	1.026	0.997
Fe_2O_3	1.688	0.363
TiO_2	0.686	0.063
$(PO_4)^{3-}$	0.013	0.013
NiO	0.012	0.012
CaO	0.117	
K	0.262	
MgO	0.288	
MnO	0.021	
Na	0.013	

[a]SiO_2 was determined by gravimetric analyses. Only metals and oxide metals were determined. The analytical technique has 1.0% of error.

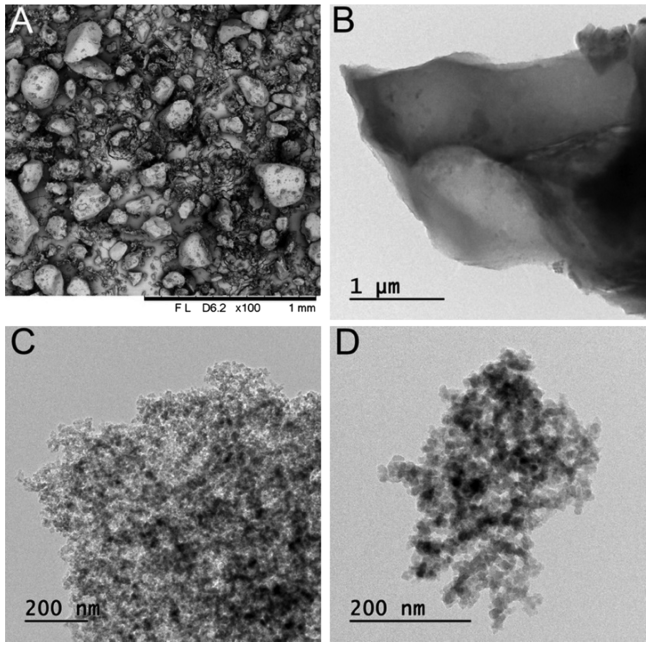

Figure 1. SWA: (A) SEM image and (B) TEM image. Silica nanoparticle TEM images with two different magnifications in (C,D).

ICP−OES is an analytical technique capable of detecting trace metals and elements in high concentrations; the weight percentage of Si was determined by classical gravimetric analyses,[34] whereas the other elements were analyzed directly by ICP−OES. The content of SiO_2 determined in sugarcane ash was 88.68 ± 0.87 wt % and in the prepared SiO_2NPs was 99.08 ± 0.99 wt %. These results demonstrate a significant purification of sample that generates high pure SiO_2NPs. The amount of Al_2O_3 decreased from 1.026 wt % (ash) to 0.997 wt % (silica), which is a slight decrease compared to Fe_2O_3, from 1.688 wt % (ash) to 0.363 wt % (silica) and TiO_2, from 0.686 wt % (ash) to 0.063 wt % (silica). The amount of $(PO_4)^{3-}$ and NiO was the same for ash and silica samples.

DOI: 10.1021/acsomega.8b00092
ACS Omega 2018, 3, 2618−2627

The elements CaO, K, MgO, MnO, and Na, which were present in the ash and were absent from the SiO_2NPs. High purity of SiO_2NPs was also observed in energy dispersive spectroscopy (EDS) analyses (Figure S1), as shown in the Supporting Information.

The SEM image of SWA shown in Figure 1A reveals a heterogeneous material with irregular shapes. Sizes between 5 and 500 μm and a high roughness were observed, which are associated with the release of organic matter during the bagasse burning process for the generation of energy in the sugar-alcohol industry. The morphologies obtained from the SWA sample are similar to those observed by Batra et al.[35] and Faria et al.[36] Figure 1B shows a TEM image of a single ash; its relatively big size makes it difficult to be analyzed by TEM.

In contrast, Figure 1C,D shows TEM images of the SiO_2NPs obtained; a drastic alteration of the material size and form prepared can be observed compared to the original ash. The size range from several micrometers for ash decreases to less than 20 nm for SiO_2NPs, but nanoparticles with a large distribution of size are not observed. However, no defined form is observed for synthesized nanoparticles, but it is possible to see that they do not present nanoparticles bigger than 50 nm, which is very similar to the size of the SiO_2NPs reported by Rafiee et al.,[37] Hassan et al.,[38] Le et al.,[39] Bahrami et al.,[40] and To et al.,[41] for SiO_2NPs obtained from rice husk.

Therefore, this method, using a micellar environment in the process of synthesis of nanoparticles, is very effective to control the size; nevertheless, nonuniform SiO_2NPs were generated. However, these results demonstrate that nanoparticles made of silica from SWA produce nanoparticles with the same form as others produced from rice husk or commercial reactants.[40−42]

The crystallographic properties of SWA also change when compared to SiO_2NPs, as shown in Figure 2. The X-ray

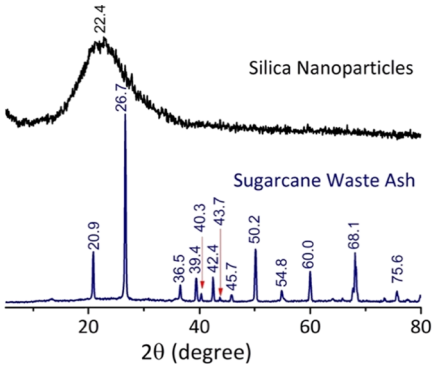

Figure 2. X-ray diffraction analyses (XRD) patterns of the SWA (blue) and SiO_2NPs (black) samples.

diffraction pattern of the SWA shows only peaks relative to crystalline silica, being very similar to the quartz pattern, whereas SiO_2NPs have a pattern that is very similar to amorphous silica.[43,44] In fact, when an organic material with a high percentage of silicon is burned, as reported for sugarcane waste, with the aim of generating energy, it can generate amorphous or crystalline silica; high temperatures (900−1000 °C) generate crystalline silica, while quartz in a crystalline form is formed in the case of SWA.[45]

The synthesis of SiO_2NPs generates amorphous silica, as can be seen by a band with a maximum peak at $\theta = 22°$,[43] while the crystalline form of silica can be highly toxic, promoting silicosis; the amorphous form is almost inoffensive, being even used for drug delivery,[21] which provides another possible application for the obtained SiO_2NPs.

As already mentioned, SiO_2NPs (Figure 1C,D) have a size that is much smaller than SWA (Figure 1A,B); consequently, a significant increase of the specific surface area is expected, which confirmed by Brunauer−Emmett−Teller (BET) analyses as shown in Figure 3.

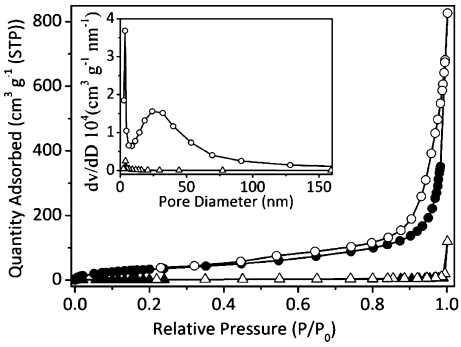

Figure 3. N_2 adsorption−desorption isotherms of the SWA (▲ adsorption and △ desorption) and SiO_2NPs (● adsorption and ○ desorption) samples. Inset: Pore size distribution of the SWA (△) and silica nanoparticle samples (○).

In the BET measurements, an isotherm type II can be observed for the SiO_2NPs with a hysteresis of H3 type, associated to slit-shaped pores formed by aggregates of platelike particles, resulting in a large pore size distribution, that is, type IIb isotherm.[46,47] The absence of a plateau in the relative pressure close to 1 in the SiO_2NPs isotherm shows the presence of macropores, and the hysteresis loop observed between the adsorption−desorption branches is the indication of mesopores.[46−49] The sugarcane ash isotherm, in turn, has isotherm type III, because of a weak adsorbent−adsorbate interaction. The absence of hysteresis loop between the adsorption−desorption branches in the SWA isotherm indicates the absence of mesopores. Therefore, the mesoporous structure of the SiO_2NPs was evaluated through the Barrett−Joyner−Halenda (BJH) method (inset in Figure 3).

In Figure 3 (inset), in the N_2 adsorption−desorption isotherm results, a wide pore size distribution between 7 and 50 nm can be observed for the SiO_2NPs sample, which indicates mesoporous materials, along with a small distribution of pores above 50 nm, which also suggests the presence of macroporous materials in the structure of nanoparticles.

Thus, these results suggest the coexistence of mesopores and macropores. The average pore diameter from the desorption isotherm branch of SiO_2NPs was 22 nm (mesoporous materials), as calculated by the BJH model (Table 2). However, the SWA sample presented only a microporous structure, because it did not present the distribution of pores above 2 nm.

Table 2. Experimental Textural Properties of the Sugarcane Waste Ash and Silica Nanoparticle Samples

sample	surface area[a] (m^2 g^{-1})	pore diameter[b] (nm)	pore volume[b] (cm^3g^{-1})
ash	5.9		0.030
SiO_2NPs	131	22	1.045

[a]BET method. [b]BJH method.

DOI: 10.1021/acsomega.8b00092
ACS Omega 2018, 3, 2618−2627

The textural properties of the SWA and silica nanoparticle samples are reported in Table 2. The specific surface area of samples was calculated by the BET method, and the average pore diameter and pore volume were calculated by the BJH method. The surface area and pore volume of SiO_2NPs were about 23 and 35 times larger than the values found for the SWA, respectively.

The pore volume and surface area of SiO_2NPs in this study are higher than those found by Yan et al.,[50] where wet-SiO_2 sample was dried by a method similar to that used here. The SiO_2NPs surface area was similar to that reported by Affandi et al.,[51] and Bahrami et al.[40] for silica obtained from bagasse ash and rice husk ash, respectively.

Adsorption Study of the SiO_2NPs Adsorbent. The adsorption of pollutants is one of the most common applications of SiO_2NPs; this material has been extensively utilized to adsorb heavy metals, emerging pollutants, dyes, and others, in drinking water.[52−54] The adsorption kinetics study can provide multiple information about the velocity of adsorption, the mechanism involved in binding to the adsorbent, and the adsorption capacity of the material. In this case was utilized acid orange 8, an azo dye, as shown in Figure 4.

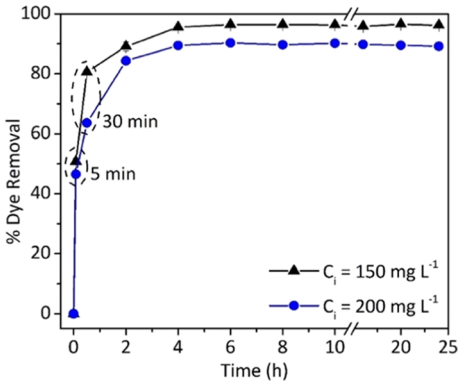

Figure 4. Effect of time on removal of acid orange 8 by silica nanoparticle adsorbent. Conditions: 25 °C; initial concentration: 150 and 200 mg L^{-1}; adsorbent mass: 1.0 g L^{-1}.

Figure 4 presents the effect of AO8 adsorption as a function of time, in terms of percentage of AO8 removed, for two initial concentrations of the dye. It was observed that the removal percentage in 5 min was around 46 and 50% for C_i = 200 and 150 mg L^{-1}, respectively, while the removal percentage in 30 min was around 63 and 80% for C_i = 200 and 150 mg L^{-1}, respectively.

The adsorption capacity was constant only after 4 h, where the removal percentage was around 89 and 95% for C_i = 200 and 150 mg L^{-1}, respectively.

The velocity of adsorption depends, generically, of physicochemical characteristics of the adsorbate, adsorbent, and solution; in this case, CTAB (the stabilizer) plays an important role. Considering the methodology utilized, it is expected to find CTAB on the surface of the nanoparticles, which worked as an agent of size control in the synthetic procedure and as a stabilizer, as can be seen in other publications.[21,23]

This surfactant has a positive charge and therefore shows affinity for anionic species, as AO8 at pH ≈ 5, the pH of deionized water, is utilized in an adsorption study. This negative charge in AO8 comes from the sulfonate group (R-SO_3^-) present in the structure, which has a pK_a lower than—2.[55]

However, the electrostatic mechanism is not the only interaction expected between AO8 and SiO_2NPs, CTAB has a long alkyl chain with 16 aliphatic carbons, generating hydrophobic regions around the surface of the nanoparticles. AO8, in turn, has three aromatic rings in its structure, with two being connected naphthalene-like, suggesting a polar molecule with nonpolar regions. These characteristics of AO8 suggest the possibility of $\pi-\pi$ packing among the molecules and, consequently, the formation of multilayers in the process of adsorption.

The presence of both molecules CTAB and AO8, on the surface of the SiO_2NPs, can be observed by Fourier transform infrared spectroscopy (FTIR), as can be seen in Figure 5, where the IR spectra of SiO_2NPs, AO8 dye, and SiO_2NPs after AO8 adsorption are presented.[55]

Analyzing every component separately, Figure 5a presents the FTIR spectrum of SiO_2NPs, where the presence of four main bands of silica is observed; at 799 and 446 cm^{-1}, the bands correlate with symmetric stretching of siloxane groups (Si−O−Si), the very strong band at 1058 cm^{-1} is assigned to Si−O−Si asymmetric stretching, and that at 965 cm^{-1} is due to OH bending, from silanol groups.

Bands related to the presence of CTAB are observed on SiO_2NPs, at 2850 and 2922 cm^{-1}, due to CH_2 symmetric and asymmetric stretching, respectively.[8,11,56−58]

Figure 5b shows the spectrum of AO8, where peaks between 1660 and 375 cm^{-1} are observed; however, no peak around 2900 cm^{-1} appears, enabling the AO8 signals of CTAB to be distinguished.

Figure 5c shows the spectrum of SiO_2NPs after AO8 adsorption, where intense peaks of silica are observed, along with less intense bands of organic molecules. It is possible to observe the peaks of CTAB around 2900 cm^{-1} and the peaks of AO8 with lower intensity between 1660 and 375 cm^{-1}. Some regions of the spectra in Figure 5 were expanded; in these expansions, it is not possible to observe apparent shifts of peaks, which suggests a nonchemical interaction between SiO_2NPs and AO8; however, it is possible to see a mixing of vibrational modes of each species, that is, special spectrum (c) shows vibrational modes of silica overlaying AO8 modes. The assignment of all peaks can be observed in Table S1.

The interaction between CTAB and AO8 can be also investigated utilizing thermogravimetric analyses (TGA). TGA can be used to quantify organic/inorganic materials present in a sample as well to distinguish the presence of different materials or to observe alterations in the thermal behavior of species when they interact with a surface. We were able to observe these points in our study. Figure 6 shows TG and derivative TG (DTG) curves of CTAB, SiO_2NPs, SiO_2NPs after AO8 adsorption and AO8 dye (see Tables S2−S4 and Figure S2).

The TG curve of CTAB (Figure 6A) shows a significant weight loss between 180 and 300 °C (86.55%, DTG at 239 °C) and a second loss between 300 and 490 °C (12.41%, DTG at 435 °C), leaving 1.04% of residue and inorganic impurities related to the purity of reactant purchased.

As already shown by FTIR spectra, SiO_2NPs have CTAB on their surface, and the TGA curve for SiO_2NPs (Figure 6B) shows this CTAB decomposition at a higher temperature, when it is bound to the SiO_2NPs (DTG at 256 °C) than isolated CTAB (DTG at 239 °C). This increase in the decomposing

DOI: 10.1021/acsomega.8b00092
ACS Omega 2018, 3, 2618−2627

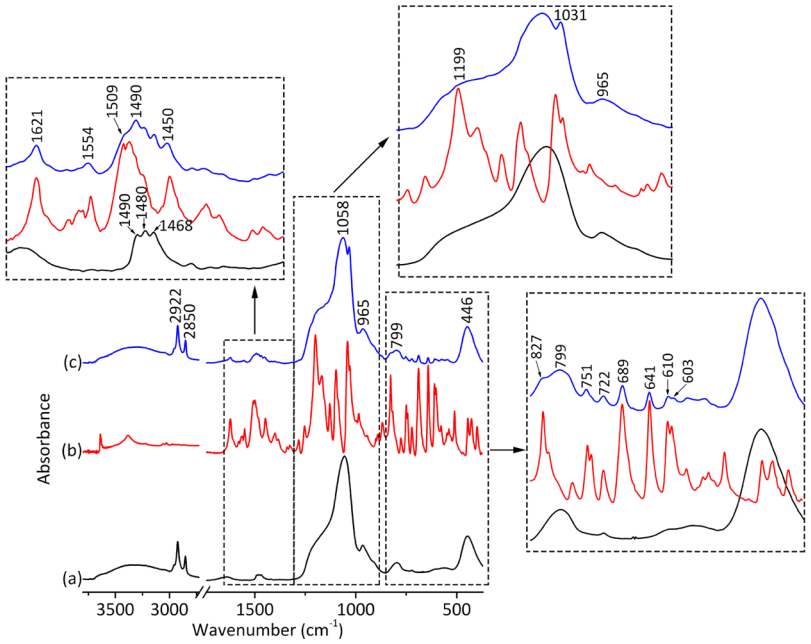

Figure 5. FTIR–attenuated total reflectance (ATR) spectra of the (a) SiO_2NPs, (b) acid orange 8 dye, and (c) SiO_2NPs + AO8 dye C_i = 200 mg L^{-1}. Inset: Regions of the spectrum of dye adsorption on SiO_2NPs.

temperature is related to a higher thermal stabilization of the molecules by electrostatic charges pairing between CTAB and the SiO_2 surface. Figure 6B also shows the unbound CTAB on the silica surface (DTG at 215 °C) due to hydrophobic–hydrophobic interactions of interconnected CTAB; both effects have already been observed in other publications.[59]

After the complete decomposition of organic material on the surface of SiO_2NPs, a residue of 64.74% was obtained, as can be seen in Figure 6B.

Two different behaviors can be highlighted in the TGA curves of the interaction between SiO_2NPs with different concentrations of AO8. First, it is possible to see a shift in DTG band at 256 °C to high temperatures, with the increase in the concentration of AO8 (Figure 6C–G); this can be explained by analyzing the DTG of AO8 dye pure (Figure 6H). AO8 shows a weight loss at 327 °C, which influences the weight loss related to CTAB, making the DTG band shift to higher temperatures, where the loss observed an average of both molecules.

The second point is related to the mass residue of the sample after AO8 adsorption; for SiO_2NPs (Figure 6B) without AO8, a final residue of inorganic material (SiO_2) of 64,74% was observed, after the adsorption of AO8 solution at a concentration of 50 mg L^{-1}, which increases to 69.95% (Figure 6C), suggesting the presence of less organic materials and, consequently, a relative larger quantity of SiO_2. The quantity of inorganic residue decreases with increasing amount of AO8 adsorbed; all of the results obtained are presented in Table S2.

These TGA results show an initial substitution of CTAB weakly binding to the nanoparticle surface by AO8.[59] This initial decrease indicates that each molecule of AO8 replaces more than one CTAB, which is a linear replacement until C_i = 100 mg L^{-1} (63.97% of residue), when it starts to form multilayers of dye saturating the surface after 200 mg L^{-1}.

This mechanism of multilayer formation proposed by TGA results agrees with kinetic results, presented in Figure 7 (see Figures S5 and S6), and the isotherm results, presented in Figure 8 (see Figure S7), both calculated by UV–visible spectroscopy, utilizing the peak with λ_{max} = 489 nm.

Figure 7 presents the kinetic results of the adsorption of a solution of AO8 in an initial concentration of 200 mg L^{-1} at 25 °C from 0 to 24 h. It is possible to observe that AO8 adsorption occurs very fast in the first hour, with 65% of dye being adsorbed, and saturation occurring after 4 h. Considering the kinetic models tested, pseudo first-order, and pseudo second-order (details of the equation are presented in Supporting Information in eqs S1 and S2), it is possible to observe a better adjustment to the pseudo second-order model (see Figure S6 and Table S5).

Kinetic models are important for describing the mechanism associated with the process of adsorption of the analyte to the adsorbent and are not associated with stoichiometry in the system.[60]

A pseudo first-order model depends basically on the analyte concentration and temperature. A pseudo second-order model, according to the model proposed by Ho and McKay,[61] applied to the process of adsorption/chemisorption, depends not only on the process of binding the analyte to the adsorbent but also to the diffusion of this analyte in the particle and/or film, which indicates the organization of the analyte on the surface of the particle. In our case, this process can be related to the process of the formation of multilayers on the surface of the nanoparticle. The calculated q_e values were close to those found experimentally (Table S5).

Adsorption isotherms, in turn, describe the relationship between the amount of the adsorbate adsorbed by the adsorbent (q_e) and the concentration of the adsorbate remaining in the solution after the system reaches equilibrium (C_e) at a constant temperature. In this study, the Langmuir,[62] Freundlich,[63] and Liu[60] isothermal models are presented in the inset of Figure 8. On the basis of the isotherm parameters of Table S6, the Liu model presented the best values of coefficient of determination adjusted ($R_{adj.}^2$), confirming that this is the

DOI: 10.1021/acsomega.8b00092
ACS Omega 2018, 3, 2618–2627

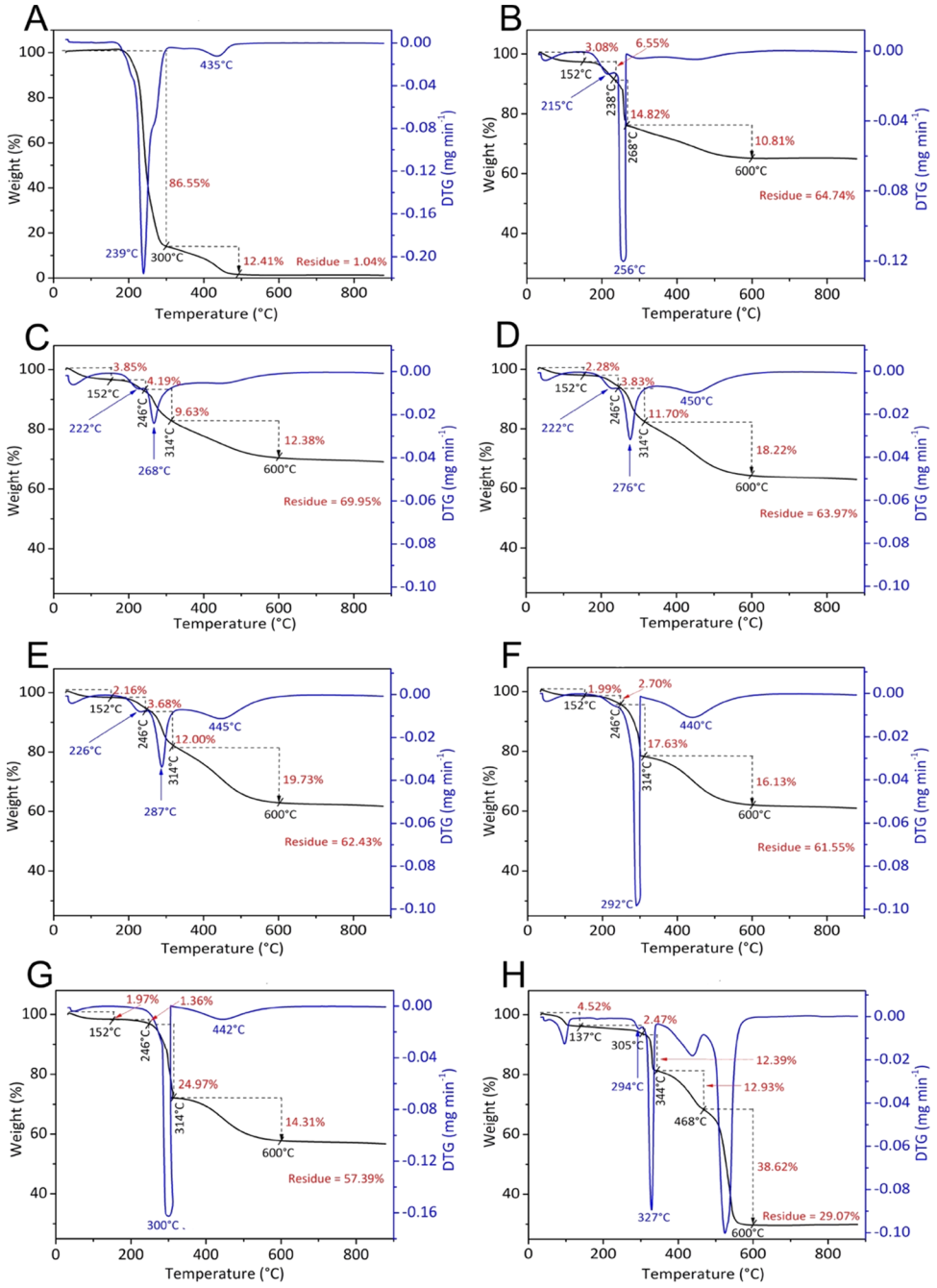

Figure 6. TG and DTG curves of (A) CTAB, (B) SiO_2NPs, (C) SiO_2NPs + AO8 (C_i = 50 mg L^{-1}), (D) SiO_2NPs + AO8 (C_i = 100 mg L^{-1}), (E) SiO_2NPs + AO8 (C_i = 150 mg L^{-1}), (F) SiO_2NPs + AO8 (C_i = 200 mg $^{-1}$), (G) SiO_2NPs + AO8 (C_i = 400 mg L^{-1}), and (H) AO8 dye. The measures were performed under an oxygen atmosphere.

best model to explain the equilibrium adsorption of AO8 by the silica nanoparticle adsorbent.

While the Langmuir model is an excellent model applied for processes involving formation of monolayers of molecules on the surface of particles/films in a finite and defined number of adsorption sites, the Freundlich model has a better application for nonhomogenous processes, over heterogeneous surfaces, and is not limited to monolayers or any uniform distribution. Finally, the Liu model can be applied to a system which has characteristics of both systems before cited.

In the model proposed by Liu, the active sites on the adsorbent do not have the same energy, which makes the adsorbent a preferential site for adsorption, leading to saturation, different to that which occurs in the Freundlich isotherm model.[64]

In our case, the Liu model shows a better plot than the other models (Figure 8, inset), which indicates the formation of multilayers of AO8 over SiO_2NPs, as well as a plateau, suggesting the saturation of adsorption. Figure 8 also presents a temperature effect in the process of adsorption, it is possible to see a relative increase in the capacity with an increase in the temperature, indicating an endothermic process, as reported in other publications.[46]

Finally, the recycling of SiO_2NPs was tested, aiming to evaluate how many times it could be used until its adsorption capacity is lost. As observed in Figure 9, SiO_2NPs can be used

DOI: 10.1021/acsomega.8b00092
ACS Omega 2018, 3, 2618−2627

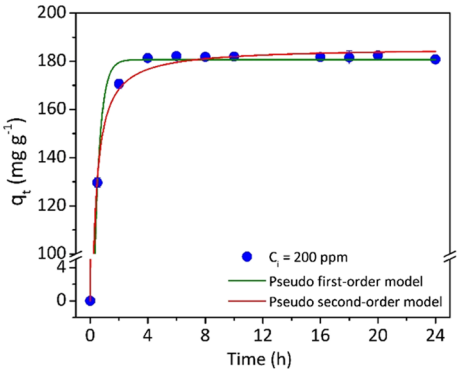

Figure 7. Pseudo first-order and pseudo second-order model kinetics plot for the removal of AO8 by the silica nanoparticle adsorbent. Conditions: 25 °C; initial concentration: 200 mg L^{-1}; adsorbent mass: 1.0 g L^{-1}.

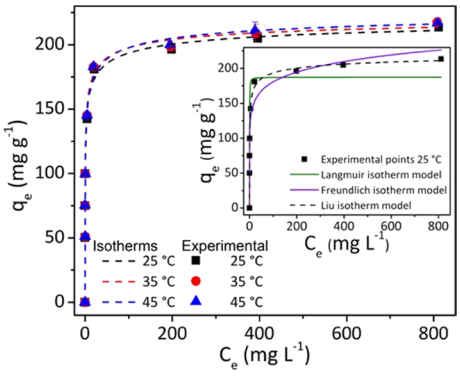

Figure 8. Adsorption Liu isotherms for AO8 adsorbed by SiO_2NPs. Conditions: 25, 35, and 45 °C; time: 4 h; adsorbent mass: 1.0 g L^{-1}. Inset: Different models of isotherms plotted for experimental data obtained at 25 °C.

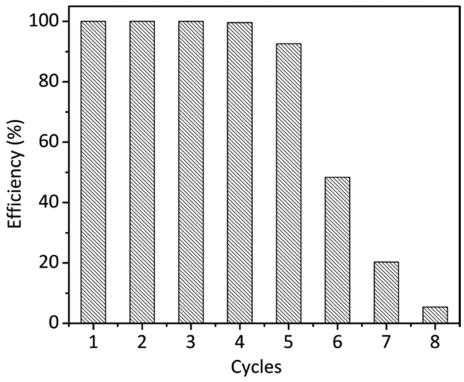

Figure 9. Recycling of SiO_2NPs after AO8 adsorption, C_i = 20 mg L^{-1} at 25 °C for 2 h (see Figures S8 and S9).

up to five times, adsorbing more than 90% of AO8; after five times, its capacity decays exponentially, possibly due to the partial removal of CTAB on the surface of nanoparticles because of the process of adsorption and the isolation of nanoparticles.[59]

Nevertheless, these results were shown to be adequate for this material to be inexpensive and indicate the possible utilization of these nanoparticles to concentrate analytes in low concentrations, opening up the possibility to utilize solid phase extraction cartridges, filters, or other materials, aimed at remediation or analytical applications.

CONCLUSIONS

This study utilized SWA for the first time, to successfully produce SiO_2NPs, and this process generated nanoparticles with high purity (>99% of SiO_2). In the preparation, cetyltrimethylammonium bromide was utilized as a stabilizer and size-controller. SiO_2NPs were characterized by TEM, which showed the presence of very small nanoparticles (<20 nm), and by the BET method, which presented a specific surface area of 131 m^2 g^{-1}, about 23 times higher than the raw sugarcane ash. Kinetic and isotherm results, in addition to thermogravimetric analyses, indicated that AO8 adsorbed to SiO_2NPs, forming multiple layers. Furthermore, the SiO_2NPs showed great adsorption capacity, around 230 mg g^{-1} and with the possibility of reuse, making it possible to reuse this for up to five cycles, adsorbing more than 90%. The results indicate that it was possible to obtain a good green adsorbent, from a renewable source, at low cost. Besides the application as an adsorbent material, these highly pure SiO_2NPs have the potential for application in catalysts, biopolymers, paints, among others.

EXPERIMENTAL SECTION

Chemicals. All aqueous solutions were prepared using deionized water (resistivity > 18.2 MΩ cm) obtained from a Milli-Q deionizer (Elix Millipore). SWA, utilized in this study, was donated by Cosan S. A., Brazil. Sodium hydroxide micropearls (>99%), hydrochloric acid (35−37%), and *n*-butyl alcohol (>99%) were purchased from Synth, Brazil. Sulfuric acid (95−97%) and CTAB (≥98%) were purchased from Merck, Germany. Acid orange 8 (AO8) dye (65%) was purchased from Aldrich, United States of America.

Characterization. The chemical compositions of SWA and SiO_2NPs were analyzed gravimetrically (for Si composition) and by ICP−OES. Briefly, silica composition was determined adapting the procedure from the literature,[34] where 100 mg of the sample (SWA or SiO_2NPs) was placed in a melting pot and calcined at 1000 °C; this sample was titrated with hydrofluoric acid, until complete dissolution of silica, and evaporated; and SiO_2 was estimated using the residual mass. The other elements were determined by ICP−OES, model Spectro Arcos from Ametek. SEM images were recorded on a tabletop microscope from Hitachi, model TM3030, at a typical acceleration voltage of 5.0 kV. TEM images were registered using a microscope from JEOL, model-JEM-2100. TEM samples were prepared by dispersing a small amount of sample in water (∼1 g L^{-1}) and sonicated in high shear, and then, 1 μL of suspension was placed onto a copper grid covered by a carbon thin film and dried in air. XRD were performed using a diffractometer Rigaku Multiflex with a Cu anode using Co Kα radiation at 40.0 kV and 20.0 mA over the range (2θ) of 5−80° with a scan time of 0.5° min^{-1}. The specific surface area and pore distribution of samples were analyzed by N_2 adsorption−desorption isotherms at −196 °C using a Micromeritics ASAP 2000 instrument. UV−visible spectra of the samples were obtained in a spectrophotometer Varian, model Cary 1E, using quartz cuvettes with a 1.0 cm path length and scanning sample from 200 to 600 nm. FTIR was performed using a spectrometer from Bruker, model Alpha, operating in ATR mode. The spectra were obtained using 200 cumulative scans, range 375−4000 cm^{-1}. Thermog-

DOI: 10.1021/acsomega.8b00092
ACS Omega 2018, 3, 2618−2627

ravimetric analyses were recorded in a thermogravimetric analyzer TGA/SDTA from Mettler Toledo. Then, ∼10.0 mg was weighed and analyzed under an oxygen atmosphere with a flow of 50.0 mL min^{-1}, using an alumina-port sample heated to 900 °C with a heating rate of 10 °C min^{-1}. To obtain TG curves of SiO_2NPs after an interaction with AO8, the nanoparticles were isolated by centrifugation, dried for 5 h at 100 °C, and analyzed. All curves were obtained under the oxygen atmosphere.

Pretreatment of the SWA. Around 200 g of SWA was added to 1000 mL of 0.10 mol L^{-1} HCl and kept under shaking for 2 h. The suspension was then filtered and washed with deionized water. The solid was oven-dried at 120 °C overnight, the SWA was sieved (particles ≤ 0.60 mm), and the fraction with smaller particles was saved.[28]

Preparation of Sodium Silicate Solution from SWA. The washed SWA was mixed with NaOH solid (1:1.5, w/w) and heated in a muffle at 400 °C for 1 h. Then, 100 mL of deionized water was added to the mixture and refluxed for 4 h. Then, the mixture was filtered to separate the solid residue of the sodium silicate (Na_2SiO_3) solution.[29,33,37,38] This procedure is illustrated in Scheme S1, Supporting Information.

Surfactant-Mediated Synthesis of SiO_2NPs from the Obtained Sodium Silicate. Utilizing a 500 mL round bottom flask, 4.5 g of CTAB was dissolved in a mixture composed of 100 mL of water and 100 mL of butyl alcohol (1:1, v/v) and heated to 60 °C. To this emulsion/biphasic system, 40 mL of sodium silicate solution obtained previously was added, under constant stirring. Finally, a 0.5 mol L^{-1} sulfuric acid solution was added to this solution, dropwise, until the pH decreased to 4, and the resulting gel was aged at 60 °C for 8 h. The aged SiO_2NPs in the gel were washed with distilled water, filtered, and oven-dried at 120 °C.[39] This procedure is illustrated in Scheme S2, Supporting Information.

Adsorption Study. The adsorption studies of AO8 dye were conducted at different initial dye concentrations, ranging from 50 to 1000 mg L^{-1}. The experiments in batch were performed at 25, 35, and 45 °C. SiO_2NPs samples (adsorbent dose = 1.0 g L^{-1}) were added to the dye solution and shaken at 100 rpm for different times from 0 to 24 h. All experiments were performed in triplicate. Analytical curves (Figure S10) were prepared to follow the analysis of aqueous solutions containing known amounts of the analyte standard. The concentration of AO8 was determined by using a UV−visible spectrophotometer at its maximum absorbance wavelength (489 nm). To measure the absorbance of samples after adsorption, they were centrifuged at 1560 G, the supernatant was removed, and then, their absorbance was measured. The amount of dye removal was expressed as the removal percentage of AO8 and calculated by eq 1

$$\%\ \text{removal} = \frac{(C_i - C_f)}{C_i} \times 100 \quad (1)$$

where C_i and C_f are the initial and final concentration of AO8, respectively. The amount of AO8 adsorption as a function of time and at equilibrium, q_t and q_e (mg g^{-1}), respectively, were calculated using the following eqs 2 and 3

$$q_e = \frac{(C_i - C_e)}{m} \times V \quad (2)$$

$$q_t = \frac{(C_i - C_f)}{m} \times V \quad (3)$$

where C_i, C_f, and C_e (mg L^{-1}) are concentrations of AO8 at initial, final, and equilibrium, respectively, V (L) is the volume of AO8 solution, and m (g) is the mass of the adsorbent.[65] Recyclability experiments were performed, similarly to the adsorption studies, using the same SiO_2NPs sample repeatedly, renewing dye solution with constant concentration.

■ ASSOCIATED CONTENT

Supporting Information

The Supporting Information is available free of charge on the ACS Publications website at DOI: 10.1021/acsomega.8b00092.

Analytical curves, chemical structure and physical−chemical properties of acid orange 8, kinetic and equilibrium adsorption models, EDS and TEM, assignments IR vibrations, additional TG, UV−vis spectra before and after the adsorption study, kinetic and equilibrium adsorption results, SiO_2NPs reuse cycles, preparation of sodium silicate from SWA, and synthesis of SiO_2NPs (PDF).

■ AUTHOR INFORMATION

Corresponding Author

*E-mail: jonnatan@iq.usp.br. Phone: +55-11-2648-1376 (J.J.S.).

ORCID

Jonnatan J. Santos: 0000-0003-3789-6229

Author Contributions

S.R. and J.J.S. contributed equally. All authors have given approval to the final version of the manuscript.

Notes

The authors declare no competing financial interest.

■ ACKNOWLEDGMENTS

We would like to thank CAPES (Coordenação de Aperfeiçoamento de Pessoal de Nível Superior), CNPq (Conselho Nacional de Desenvolvimento Científico e Tecnológico), and FAPESP (Fundação de Amparo à Pesquisa do Estado de São Paulo) for financial support. We also thank Dr. Ricardo Couto and Profª. Vera R. L. Constantino, from IQ-USP, for BET analyses, Dra. Duclerc F. Parra for TG analyses, and Dra. Nilce Ortiz for making the UV−visible spectrophotometer available to collect UV−vis spectra and acknowledge COSAN S.A. (São Paulo, Brazil) for supplying the sugarcane waste ash.

■ REFERENCES

(1) Didaskalou, C.; Buyuktiryaki, S.; Kecili, R.; Fonte, C. P.; Szekely, G. Valorisation of agricultural waste with an adsorption/nanofiltration hybrid process: from materials to sustainable process design. *Green Chem.* **2017**, *19*, 3116−3125.

(2) Arshadi, M.; Attard, T. M.; Lukasik, R. M.; Brncic, M.; da Costa Lopes, A. M.; Finell, M.; Geladi, P.; Gerschenson, L. N.; Gogus, F.; Herrero, M.; Hunt, A. J.; Ibáñez, E.; Kamm, B.; Mateos-Aparicio, I.; Matias, A.; Mavroudis, N. E.; Montoneri, E.; Morais, A. R. C.; Nilsson, C.; Papaioannou, E. H.; Richel, A.; Rupérez, P.; Škrbić, B.; Solarov, M. B.; Švarc-Gajić, J.; Waldron, K. W.; Yuste-Córdoba, F. J. Pre-treatment and extraction techniques for recovery of added value compounds from wastes throughout the agri-food chain. *Green Chem.* **2016**, *18*, 6160−6204.

(3) Marion, P.; Bernela, B.; Piccirilli, A.; Estrine, B.; Patouillard, N.; Guilbot, J.; Jérôme, F. Sustainable chemistry: how to produce better and more from less? *Green Chem.* **2017**, *19*, 4973−4989.

DOI: 10.1021/acsomega.8b00092
ACS Omega 2018, 3, 2618−2627

(4) Vaibhav, V.; Vijayalakshmi, U.; Roopan, S. M. Agricultural waste as a source for the production of silica nanoparticles. *Spectrochim. Acta, Part A* **2015**, *139*, 515−520.
(5) Noor-ul-Amin. A multi-directional utilization of different ashes. *RSC Adv.* **2014**, *4*, 62769−62788.
(6) Carmona, V. B.; Oliveira, R. M.; Silva, W. T. L.; Mattoso, L. H. C.; Marconcini, J. M. Nanosilica from rice husk: Extraction and characterization. *Ind. Crops Prod.* **2013**, *43*, 291−296.
(7) Chen, H.; Wang, W.; Martin, J. C.; Oliphant, A. J.; Doerr, P. A.; Xu, J. F.; DeBorn, K. M.; Chen, C.; Sun, L. Extraction of Lignocellulose and Synthesis of Porous Silica Nanoparticles from Rice Husks: A Comprehensive Utilization of Rice Husk Biomass. *ACS Sustainable Chem. Eng.* **2013**, *1*, 254−259.
(8) Hu, S.; Hsieh, Y.-L. Preparation of Activated Carbon and Silica Particles from Rice Straw. *ACS Sustainable Chem. Eng.* **2014**, *2*, 726−734.
(9) Alshatwi, A. A.; Athinarayanan, J.; Periasamy, V. S. Biocompatibility assessment of rice husk-derived biogenic silica nanoparticles for biomedical applications. *Mater. Sci. Eng., C* **2015**, *47*, 8−16.
(10) Wang, Z.; Liu, J.; Wang, W.; Wei, Z.; Wang, F.; Gong, P.; Wang, J.; Li, N.; Liu, B.; Zhang, Z.; Wang, W.; Sun, L. Photoluminescent carbon quantum dot grafted silica nanoparticles directly synthesized from rice husk biomass. *J. Mater. Chem. B* **2017**, *5*, 4679−4689.
(11) Boza, A. F.; Kupfer, V. L.; Oliveira, A. R.; Radovanovic, E.; Rinaldi, A. W.; Meneguin, J. G.; Domingues, N. L. C.; Moisés, M. P.; Favaro, S. L. Synthesis of α-aminophosphonates using a mesoporous silica catalyst produced from sugarcane bagasse ash. *RSC Adv.* **2016**, *6*, 23981−23986.
(12) Arumugam, A.; Ponnusami, V. Synthesis of SBA-15 from low cost silica precursor obtained from sugarcane leaf ash and its application as a support matrix for lipase in biodiesel production. *J. Sol-Gel Sci. Technol.* **2013**, *67*, 244−250.
(13) Luca, E. F.; Chaplot, V.; Mutema, M.; Feller, C.; Ferreira, M. L.; Cerri, C. C.; Couto, H. T. Z. Effect of conversion from sugarcane preharvest burning to residues green-trashing on SOC stocks and soil fertility status: Results from different soil conditions in Brazil. *Geoderma* **2018**, *310*, 238−248.
(14) CONAB (Companhia Nacional de Abastecimento), 2017. Acompanhamento da safra brasileira: cana de açúcar: safra 2016/2017 − quarto levantamento, abril/2017. Brasilia. Accessed at <http://www.conab.gov.br//> on 26 Out 2017.
(15) Norsuraya, S.; Fazlena, H.; Norhasyimi, R. Sugarcane Bagasse as a Renewable Source of Silica to Synthesize Santa Barbara Amorphous-15 (SBA-15). *Procedia Eng.* **2016**, *148*, 839−846.
(16) Mizutani, T.; Arai, K.; Miyamoto, M.; Kimura, Y. Application of silica-containing nano-composite emulsion to wall paint: A new environmentally safe paint of high performance. *Prog. Org. Coat.* **2006**, *55*, 276−283.
(17) Zhao, S.; Malfait, W. J.; Demilecamps, A.; Zhang, Y.; Brunner, S.; Huber, L.; Tingaut, P.; Rigacci, A.; Budtova, T.; Koebel, M. M. Strong, Thermally Superinsulating Biopolymer-Silica Aerogel Hybrids by Cogelation of Silicic Acid with Pectin. *Angew. Chem.* **2015**, *54*, 14282−14286.
(18) Vijayakumar, V.; Khastgir, D. Hybrid composite membranes of chitosan/sulfonated polyaniline/silica as polymer electrolyte membrane for fuel cells. *Carbohydr. Polym.* **2018**, *179*, 152−163.
(19) Wong, D. P.; Suriyaprabha, R.; Yuvakumar, R.; Rajendran, V.; Chen, Y.-T.; Hwang, B.-J.; Chen, L.-C.; Chen, K.-H. Binder-free rice husk-based silicon-graphene composite as energy efficient Li-ion battery anodes. *J. Mater. Chem. A* **2014**, *2*, 13437−13441.
(20) Sharma, R. K.; Sharma, S.; Dutta, S.; Zboril, R.; Gawande, M. B. Silica-nanosphere-based organic-inorganic hybrid nanomaterials: synthesis, functionalization and applications in catalysis. *Green Chem.* **2015**, *17*, 3207−3230.
(21) Chen, F.; Zhao, E.; Kim, T.; Wang, J.; Hableel, G.; Reardon, P. J. T.; Ananthakrishna, S. J.; Wang, T.; Arconada-Alvarez, S.; Knowles, J. C.; Jokerst, J. V. Organosilica Nanoparticles with an Intrinsic Secondary Amine: An Efficient and Reusable Adsorbent for Dyes. *ACS Appl. Mater. Interfaces* **2017**, *9*, 15566−15576.
(22) Mahmoodi, N. M.; Maghsoudi, A.; Najafi, F.; Jalili, M.; Kharrati, H. Primary-secondary amino silica nanoparticle: synthesis and dye removal from binary system. *Desalin. Water Treat.* **2014**, *52*, 7784−7796.
(23) Nayab, S.; Farrukh, A.; Oluz, Z.; Tuncel, E.; Tariq, S. R.; ur Rahman, H.; Kirchhoff, K.; Duran, H.; Yameen, B. Design and fabrication of branched polyamine functionalized mesoporous silica: an efficient absorbent for water remediation. *ACS Appl. Mater. Interfaces* **2014**, *6*, 4408−4417.
(24) Wang, Y.; Kalinina, A.; Sun, T.; Nowack, B. Probabilistic modeling of the flows and environmental risks of nano-silica. *Sci. Total Environ.* **2016**, *545*−*546*, 67−76.
(25) Kyzas, G.; Kostoglou, M. Green Adsorbents for Wastewaters: A Critical Review. *Materials* **2014**, *7*, 333−364.
(26) Gillet, S.; Aguedo, M.; Petitjean, L.; Morais, A. R. C.; da Costa Lopes, A. M.; Łukasik, R. M.; Anastas, P. T. Lignin transformations for high value applications: towards targeted modifications using green chemistry. *Green Chem.* **2017**, *19*, 4200−4233.
(27) Fan, J.; Li, D.; Teng, W.; Yang, J.; Liu, Y.; Liu, L.; Elzatahry, A. A.; Alghamdi, A.; Deng, Y.; Li, G.; Zhang, W.-x.; Zhao, D. Ordered mesoporous silica/polyvinylidene fluoride composite membranes for effective removal of water contaminants. *J. Mater. Chem. A* **2016**, *4*, 3850−3857.
(28) Kalapathy, U.; Proctor, A.; Shultz, J. A simple method for production of pure silica from rice hull ash. *Bioresour. Technol.* **2000**, *73*, 257−262.
(29) Alves, R. H.; Reis, T. V. d. S.; Rovani, S.; Fungaro, D. A. Green Synthesis and Characterization of Biosilica Produced from Sugarcane Waste Ash. *J. Chem.* **2017**, *2017*, 1−9.
(30) Kalapathy, U.; Proctor, A. A new method for free fatty acid reduction in frying oil using silicate films produced from rice hull ash. *J. Am. Oil Chem. Soc.* **2000**, *77*, 593−598.
(31) Wu, S.-H.; Mou, C.-Y.; Lin, H.-P. Synthesis of mesoporous silica nanoparticles. *Chem. Soc. Rev.* **2013**, *42*, 3862−3875.
(32) Hoffmann, F.; Cornelius, M.; Morell, J.; Fröba, M. Silica-Based Mesoporous Organic−Inorganic Hybrid Materials. *Angew. Chem., Int. Ed.* **2006**, *45*, 3216−3251.
(33) Wang, X.; Li, W.; Zhu, G.; Qiu, S.; Zhao, D.; Zhong, B. Effects of ammonia/silica molar ratio on the synthesis and structure of bimodal mesopore silica xerogel. *Microporous Mesoporous Mater.* **2004**, *71*, 87−97.
(34) Kalocsai, G. I. Z.; Hockley, J. J. Titrimetric Analysis for Silicon. *Mineral. Mag.* **1972**, *38*, 618−622.
(35) Batra, V.; Urbonaite, S.; Svensson, G. Characterization of unburned carbon in bagasse fly ash. *Fuel* **2008**, *87*, 2972−2976.
(36) Faria, K. C. P.; Gurgel, R. F.; Holanda, J. N. F. Recycling of sugarcane bagasse ash waste in the production of clay bricks. *J. Environ. Manage.* **2012**, *101*, 7−12.
(37) Rafiee, E.; Shahebrahimi, S.; Feyzi, M.; Shaterzadeh, M. Optimization of synthesis and characterization of nanosilica produced from rice husk (a common waste material). *Int. Nano Lett.* **2012**, *2*, 29.
(38) Hassan, A. F.; Abdelghny, A. M.; Elhadidy, H.; Youssef, A. M. Synthesis and characterization of high surface area nanosilica from rice husk ash by surfactant-free sol-gel method. *J. Sol-Gel Sci. Technol.* **2014**, *69*, 465−472.
(39) Le, V. H.; Thuc, C. N. H.; Thuc, H. H. Synthesis of silica nanoparticles from Vietnamese rice husk by sol-gel method. *Nanoscale Res. Lett.* **2013**, *8*, 58.
(40) Bahrami, A.; Simon, U.; Soltani, N.; Zavareh, S.; Schmidt, J.; Pech-Canul, M. I.; Gurlo, A. Eco-fabrication of hierarchical porous silica monoliths by ice-templating of rice husk ash. *Green Chem.* **2017**, *19*, 188−195.
(41) To, T. Q.; Kenny, C.; Cheong, S.; Aldous, L. Carbon dioxide as a pH-switch anti-solvent for biomass fractionation and pre-treatment with aqueous hydroxide solutions. *Green Chem.* **2017**, *19*, 2129−2134.
(42) Bachmann, C.; Probst, B.; Oberholzer, M.; Fox, T.; Alberto, R. Photocatalytic proton reduction with ruthenium and cobalt complexes immobilized on fumed reversed-phase silica. *Chem. Sci.* **2016**, *7*, 436−445.

DOI: 10.1021/acsomega.8b00092
ACS Omega 2018, 3, 2618−2627

(43) Chen, X.; Jiang, J.; Yan, F.; Tian, S.; Li, K. A novel low temperature vapor phase hydrolysis method for the production of nano-structured silica materials using silicon tetrachloride. *RSC Adv.* **2014**, *4*, 8703−8710.
(44) Rodríguez-Díaz, J. M.; García, J. O. P.; Sánchez, L. R. B.; da Silva, M. G. C.; da Silva, V. L.; Arteaga-Pérez, L. E. Comprehensive Characterization of Sugarcane Bagasse Ash for Its Use as an Adsorbent. *BioEnergy Res.* **2015**, *8*, 1885−1895.
(45) Le Blond, J. S.; Horwell, C. J.; Williamson, B. J.; Oppenheimer, C. Generation of crystalline silica from sugarcane burning. *J. Environ. Monit.* **2010**, *12*, 1459−1470.
(46) Santos, R. M. M. d.; Gonçalves, R. G. L.; Constantino, V. R. L.; Santilli, C. V.; Borges, P. D.; Tronto, J.; Pinto, F. G. Adsorption of Acid Yellow 42 dye on calcined layered double hydroxide: Effect of time, concentration, pH and temperature. *Appl. Clay Sci.* **2017**, *140*, 132−139.
(47) Rouquerol, J.; Rouquerol, F.; Sing, K. General Conclusions and Recommendations. *Absorption by Powders and Porous Solids*; Elsevier, 1998; p 467.
(48) Sing, K. S. W. Reporting physisorption data for gas/solid systems with special reference to the determination of surface area and porosity (Recommendations 1984). *Pure Appl. Chem.* **1985**, *57*, 603.
(49) Rosu, M.-C.; Suciu, R.-C.; Mihet, M.; Bratu, I. Physical-chemical characterization of titanium dioxide layers sensitized with the natural dyes carmine and morin. *Mater. Sci. Semicond. Process.* **2013**, *16*, 1551−1557.
(50) Yan, F.; Jiang, J.; Chen, X.; Tian, S.; Li, K. Synthesis and Characterization of Silica Nanoparticles Preparing by Low-Temperature Vapor-Phase Hydrolysis of SiCl4. *Ind. Eng. Chem. Res.* **2014**, *53*, 11884−11890.
(51) Affandi, S.; Setyawan, H.; Winardi, S.; Purwanto, A.; Balgis, R. A facile method for production of high-purity silica xerogels from bagasse ash. *Adv. Powder Technol.* **2009**, *20*, 468−472.
(52) Martín-de-Lucía, I.; Campos-Mañas, M. C.; Agüera, A.; Rodea-Palomares, I.; Pulido-Reyes, G.; Leganés, F.; Fernández-Piñas, F.; Rosal, R. Reverse Trojan-horse effect decreased wastewater toxicity in the presence of inorganic nanoparticles. *Environ. Sci.: Nano* **2017**, *4*, 1273−1282.
(53) Subramani, A.; Jacangelo, J. G. Emerging desalination technologies for water treatment: A critical review. *Water Res.* **2015**, *75*, 164−187.
(54) Tao, J.; Xiong, J.; Jiao, C.; Zhang, D.; Lin, H.; Chen, Y. Hybrid Mesoporous Silica Based on Hyperbranch-Substrate Nanonetwork as Highly Efficient Adsorbent for Water Treatment. *ACS Sustainable Chem. Eng.* **2016**, *4*, 60−68.
(55) Konicki, W.; Aleksandrzak, M.; Moszyński, D.; Mijowska, E. Adsorption of anionic azo-dyes from aqueous solutions onto graphene oxide: Equilibrium, kinetic and thermodynamic studies. *J. Colloid Interface Sci.* **2017**, *496*, 188−200.
(56) Su, P.; Wang, R.; Yu, Y.; Yang, Y. Microwave-assisted synthesis of ionic liquid-modified silica as a sorbent for the solid-phase extraction of phenolic compounds from water. *Anal. Methods* **2014**, *6*, 704−709.
(57) Zhang, T.; Xu, G.; Puckette, J.; Blum, F. D. Effect of Silica on the Structure of Cetyltrimethylammonium Bromide. *J. Phys. Chem. C* **2012**, *116*, 11626−11634.
(58) Ruiz, Y. P.; Ferrão, M. F.; Cardoso, M. B.; Moncada, E. A.; dos Santos, J. H. Z. Structural discrimination of nanosilica particles and mixed-structure silica by multivariate analysis applied to SAXS profiles in combination with FT-IR spectroscopy. *RSC Adv.* **2016**, *6*, 72306−72316.
(59) Guan, H.; Bestland, E.; Zhu, C.; Zhu, H.; Albertsdottir, D.; Hutson, J.; Simmons, C. T.; Ginic-Markovic, M.; Tao, X.; Ellis, A. V. Variation in performance of surfactant loading and resulting nitrate removal among four selected natural zeolites. *J. Hazard. Mater.* **2010**, *183*, 616−621.
(60) Liu, Y.; Liu, Y.-J. Biosorption isotherms, kinetics and thermodynamics. *Sep. Purif. Technol.* **2008**, *61*, 229−242.
(61) Ho, Y. S.; McKay, G. Pseudo-second order model for sorption processes. *Process Biochem.* **1999**, *34*, 451−465.
(62) Langmuir, I. The Adsorption of Gases on Plane Surfaces of Glass, Mica and Platinum. *J. Am. Chem. Soc.* **1918**, *40*, 1361−1403.
(63) Freundlich, H. M. F. Over the Adsorption in Solution. *J. Phys. Chem.* **1906**, *57*, 385−471.
(64) Lima, É. C.; Adebayo, M. A.; Machado, F. M. Kinetic and Equilibrium Models of Adsorption. In *Carbon Nanomaterials as Adsorbents for Environmental and Biological Applications*; Bergmann, C. P., Machado, F. M., Eds; Springer International Publishing: Cham, 2015; pp 33−69.
(65) Rovani, S.; Rodrigues, A. G.; Medeiros, L. F.; Cataluña, R.; Lima, É. C.; Fernandes, A. N. Synthesis and characterisation of activated carbon from agroindustrial waste—Preliminary study of 17β-estradiol removal from aqueous solution. *J. Environ. Chem. Eng.* **2016**, *4*, 2128−2137.

DOI: 10.1021/acsomega.8b00092
ACS Omega 2018, 3, 2618−2627